Stochastic Environmental Research and Risk Assessment 16 (2002) 43–62 © Springer-Verlag 2002

New anisotropic covariance models and estimation of anisotropic parameters based on the covariance tensor identity

D. T. Hristopulos

Abstract. Many heterogeneous media and environmental processes are statistically anisotropic. In this paper we focus on range anisotropy, that is, stochastic processes with variograms that have direction dependent correlation lengths and direction independent sill. We distinguish between two classes of anisotropic covariance models: Class (A) models are reducible to isotropic after rotation and rescaling operations. Class (B) models can be separated into a product of one-dimensional functions oriented along the principal axes. We propose a new Class (A) model with multiscale properties that has applications in subsurface hydrology. We also present a family of Class (B) models based on non-Euclidean distance metrics that are generated by superellipsoidal functions. Next, we propose a new method for determining the orientation of the principal axes and the degree of anisotropy, i.e., the ratio(s) of the correlation lengths. This information reduces the degrees of freedom of anisotropic variograms and thus simplifies the estimation procedure. In particular, Class (A) models are reduced to isotropic and Class (B) models to one-dimensional functions. Our method is based on an explicit relation between the second-rank slope tensor (SRST), which can be estimated from the data, and the covariance tensor. The procedure is conceptually simple and numerically efficient. It is more accurate for regular (on-grid) data distributions, but it can also be used for sparse (off-grid) spatial distributions. In the case of non-differentiable random fields the method can be extended using generalized derivatives. We illustrate its implementation with numerical simulations.

Key words: Anisotropy, random fields, covariance tensor, power law, simulation.

1 Introduction

A central operation in spatial statistics is the estimation of the variogram (structure function) which quantifies the spatial dependence of geophysical and environmental processes (e.g., Christakos, 1992). Estimation of the spatial dependence is important in materials science as well, where it provides information about the microscopic structure (e.g., Chaikin and Lubensky, 1995) of nanostructured block copolymers (Jinnai et al., 2000a, b) microemulsions (Choy and Chen, 2000), and paper (e.g., Provatas et al., 1996). Spatial dependence in most natural and engineered materials shows various forms of anisotropy

D. T. Hristopulos
Pulp and Paper Research Institute of Canada,
570 St.-John Blvd., Pointe-Claire, QC, H9R 3J9, Canada
e-mail: dhristopulos@paprican.ca

(e.g., Erikson and Siska, 2000). In this work we focus on range anisotropy, which describes processes that have the same variogram sill in all directions but different correlation lengths. We propose new covariance functions that include a truncated power-law with multiscale properties, and separable covariance functions based on superellipsoids. The truncated power-law covariance is relevant for hydrological applications. The superellipsoidal functions can be used to model anisotropic processes with non-Euclidean distance metrics (Christakos et al., 2000).

In materials applications ensemble averages are calculated based on multiple samples. In contrast, the variogram of environmental processes is de facto estimated from the single available realization based on the ergodic principle (e.g., Adler, 1981). Since ergodicity is an asymptotic property a large sample is needed for good accuracy. Variogram estimation uses arbitrarily defined discrete classes (bins), each containing a range of separations (lags). A minimum number of data pairs (at least 30) are required to obtain a "good" approximation of the ensemble average. For isotropic processes the data are binned according to their separation. In the anisotropic case a larger bin number is required to account for both the magnitude and orientation of the separation vector. This reduces the number of data pairs per bin and consequently the precision of the estimate.

The estimation of anisotropic variograms is simplified in a coordinate system that reduces the anisotropy. For range anisotropic processes, such a system is obtained from the original by rotation and rescaling transformations. We propose a new method for determining these transformations based on the second-rank slope tensor (SRST) and the covariance tensor identity. The SRST method estimates the orientation of the principal axes and $d-1$ correlation aspect ratios (d being the spatial dimension) from the data. The aspect ratios are defined arbitrarily with respect to one of the correlation lengths. The orientation of the principal axes is determined from $d-1$ angles. The aspect ratios and the orientation angles constitute the anisotropic parameters. After rotation and rescaling of the coordinate system the variogram becomes isotropic for class (A) models or a product of one-dimensional functions for class (B) models. The SRST method is conceptually simple and numerically efficient, especially for data distributed on a regular grid. Application of the method is illustrated with synthetic examples on regular grids and sparse distributions.

The paper is structured as follows: In Sect. 2 we present the covariance classification and the proposed models. In Sect. 3 we introduce the covariance tensor identity and the formalism for the estimation of the anisotropic parameters. Practical methods for the estimation of the anisotropic parameters on regular grids are presented in Sect. 4, and for sparse data in Sect. 5. Sect. 6 includes conclusions and future directions.

2
Range anisotropic covariance functions

We will focus on statistically homogeneous, zero-mean Gaussian random fields $X(\mathbf{s})$. The centered covariance function is denoted by $c_x(\mathbf{h})$, where $\mathbf{h}$ is the separation vector. The limit of the covariance at zero separation is independent of the direction in which the limit is approached. However, the covariance derivatives depend on the direction due to the difference in the correlation lengths. In the SRST method we use information from the derivatives to simplify variogram estimation. Calculation of the SRST and the anisotropic parameters involves the same steps for both class (A) and (B) models.

Class (A): Models reducible to isotropic

This class includes covariances that can be expressed as isotropic functions $c_x(\tilde{r})$, where $\tilde{r}$ is the dimensionless separation in a coordinate system obtained by rotation and rescaling of the original. Rotation leads to a coordinate system aligned with the principal axes. The separation in the new system is denoted by $\mathbf{r} = \mathbf{U}\mathbf{h}$, where $\mathbf{U}$ is the rotation matrix (for isotropic covariances $\mathbf{h}$ and $\mathbf{r}$ are identical). In the new system the covariance is independent of cross products $r_i r_j$ $(i \neq j)$, but it is still anisotropic with correlation lengths ξ_i in each direction. If distances are rescaled by $\tilde{r}_i = r_i/\xi_i$, the covariance function becomes isotropic. Conversely, an isotropic function $c_x(\tilde{r})$ generates the anisotropic function $c_x(\mathbf{h})$ by reversing the rescaling and rotation transformations. Class (A) includes the standard geostatistical models (e.g., Abrahamsen, 1997): Gaussian, spherical, cubic, rational quadratic, exponential, damped sine and cosine (with inverse distance or exponential damping,) Bessel-function, and hole-effect models.

With the exception of the Bessel function models, the above covariances involve one or two distinct length scales. Such covariances are commonly used in groundwater hydrology (e.g., Gelhar, 1993) to model hydraulic conductivity and flow velocity correlations. However, natural porous media are composed of grains and pores of various sizes, and so subsurface hydrological processes should involve multiple scales (e.g., Cushman, 1984, 1986). Multiscale correlations are based on power-law functions (Mandelbrot, 1982; Feder, 1988) that follow the general expression $c_x(\mathbf{r}) \propto r^{-\nu}$ (where $r = \|\mathbf{r}\|$ is the Euclidean distance,) within a finite scaling range (e.g., Isichenko, 1992). These functions are also called scaling, because under a change of distance the function is simply multiplied with a constant scale factor, i.e., $c_x(\lambda\mathbf{r}) = \lambda^{-\nu} c_x(\mathbf{r})$. A major practical difficulty in determining whether subsurface variables have scaling dependence is the limited size of data sets. In contrast, scaling hypotheses have been established for rainfall data (e.g., Schertzer and Lovejoy, 1987; Lovejoy and Schertzer, 1995; Venezziano et al., 1996; Menadbe et al., 1999). In principle, power-law correlations can be obtained by a superposition of monoscale fluctuations with multiple scales (e.g., Koch and Brady, 1988). Experimental studies of porous rock (Makse et al., 1996a) indicate power-law correlations in the millimeter to meter range. In addition, certain analyses suggest scaling behavior for the hydraulic conductivity at the field scale (Neuman, 1990, 1994), and power-law covariances have been used to model flow and transport (e.g., Di Federico and Neuman, 1997, 1998). The type of power-law dependence is related to the degree of non-homogeneity of the hydraulic conductivity. The fractional Gaussian noise (*fGn*) and the Lévy-stable distributions (*LSD*) (Painter, 1996; Liu and Molz, 1997) are appropriate for homogeneous random fields. The *fGn* model includes Gaussian random fields with a power-law covariance. The probability densities of Lévy-stable random fields have non-Gaussian tails. For non-homogeneous fields the fractional Brownian motion (*fBm*) (Mandelbrot and Van Ness, 1968) and the fractional Lévy motion (*fLm*) (Molz et al., 1997) are more appropriate. The log-conductivity increments are in this case homogeneous and have *fGn* and *LSD* statistics respectively. The reconstruction and permeability of *fBm* porous media are investigated in (Kikkinides and Burganos, 1999, 2000).

According to Bochner's theorem (Bochner, 1959) well defined (permissible) covariances have spectral densities that are non-negative and integrable. Power laws are permissible covariances if the singularity at zero is cut off. The short-range cutoff is related to the smallest length scale present in the process (in the case of hydraulic conductivity this would be the size of the smallest pore). A

power-law covariance with short-range cutoff based on the incomplete gamma function was proposed in (Christakos et al., 2000).

At large distances, asymptotic persistence of power-law correlations is a sign of long-range dependence. If the power law persists over the system scale, the power exponent should be bounded for the spectral density to be well defined (Isichenko, 1992). Long-range correlations have a significant effect on physical processes in porous media (e.g., Bouchaud and Georges, 1990). If the scaling behavior extends up to a maximum scale, which is smaller than the system size, the long-range regime is cut off. The numerical simulation of random fields with long-range correlations that span the entire system is not trivial (e.g., Makse et al., 1996). An explicit long-range cutoff, if justified by the analysis of the data or the physics of the process, can alleviate numerical difficulties. We consider the following function, defined for $\nu > 0$

$$c_x(\mathbf{r}) = \sigma^2 \frac{\exp(-r/\xi)}{(1 + r^2/w^2)^{\nu/2}} = \sigma^2 \frac{\exp(-\rho w/\xi)}{(1+\rho^2)^{\nu/2}}, \quad \rho = r/w \ . \tag{1}$$

The spectral density of the exponential is non-negative and integrable, and the density of the rational function is non-negative and bounded (although not integrable for all values of ν). Their convolution is a non-negative and integrable function that satisfies Bochner's theorem. Since the convolution is the spectral density $\tilde{c}_x(\mathbf{k})$, the function $c_x(\mathbf{r})$ is a permissible covariance. The length w determines the short-range cutoff. For $r/w \ll 1$ the approximation $c_x(\mathbf{r}) \cong \sigma^2(1 - \nu r^2/2w^2)$ is good. The length scale ξ sets the long-range cutoff, since for $r > \xi$ the correlations are exponentially damped. The normalized distance $\rho = r/w$ is used to express the covariance in terms of a single length parameter, the ratio w/ξ. The covariance $c_x(\mathbf{r})$ behaves as a *fGn* for $w \ll r \ll \xi$, as shown on the log–log plots of Fig. 1. Within the scaling regime the plots of $c_x(\mathbf{r})$ vary as straight lines with slope $-\nu$. For comparison we also plot the

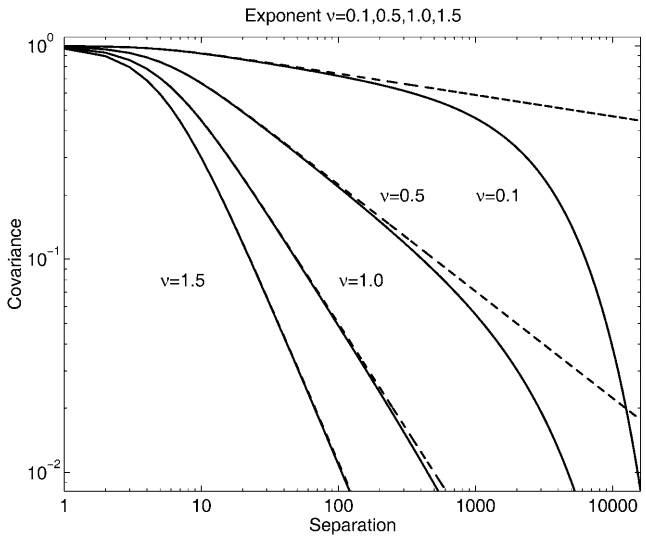

Fig. 1. Plots of the power-law covariances with short-range cutoff $w = 5$ and exponents $\nu = 0.1, 0.5, 1.0$ and 1.5. The solid curves include a long-range cutoff $\xi = 4000$, the broken-line curves have pure power law tails

unconstrained power laws. The integral scale of the covariance, defined by $\lambda = \sigma^{-2} \int_0^\infty \mathrm{d}r c_x(\mathbf{r})$, is given by

$$\lambda = \frac{w\sqrt{\pi}}{2} \left(\frac{2\xi}{w}\right)^{(1-v)/2} \Gamma(1-v/2) \left[H_{(1-v)/2}(w/\xi) - N_{(1-v)/2}(w/\xi)\right] \ , \tag{2}$$

where $H_{(1-v)/2}(w/\xi)$ is the Struve function of order $(1-v)/2$ and $N_{(1-v)/2}(w/\xi)$ the Bessel function of the second kind (Gradshteyn and Ryzhik, 1994). Since $w/\xi \ll 1$, using the leading order terms of the Struve and Bessel function expansions for $0 \leq v < 1$ we obtain

$$\frac{\lambda}{w} \cong \left(\frac{\xi}{w}\right)^{1-v} \frac{2^{-v}\sqrt{\pi}\Gamma(1-v/2)}{\sin[(1-v)\pi/2]\Gamma(1/2+v/2)} \ . \tag{3}$$

According to Eq. (3) the integral scale depends on ξ, w and v. For $v = 0$ we obtain $\lambda = \xi$ in agreement with the fact that in this case $c_x(\mathbf{r})$ is exponential. As the power exponent v increases towards one, w becomes the dominant length of the integral scale.

Anisotropic covariance models can be constructed based on Eq. (1). In the coordinate system of the principal axes they are defined as follows

$$c_x(\mathbf{r}) = \sigma^2 \frac{\exp\left(-\sqrt{\sum_{i=1}^d r_i^2/\xi_i^2}\right)}{\left(1+\sum_{i=1}^d r_i^2/w_i^2\right)^{v/2}} = \sigma^2 \frac{\exp\left(-\sqrt{\sum_{i=1}^d \rho_i^2 w_i^2/\xi_i^2}\right)}{\left(1+\sum_{i=1}^d \rho_i^2\right)^{v/2}}, \quad \rho_i = r_i/w_i \ . \tag{4}$$

The covariance (4) has anisotropic cutoffs but isotropic power exponent. A more general covariance with anisotropic exponents $v_i (i = 1, \ldots, d)$ is given by

$$c_x(\mathbf{r}) = d\sigma^2 \frac{\exp\left(-\sqrt{\sum_{i=1}^d r_i^2/\xi_i^2}\right)}{\sum_{i=1}^d \left(1+r_i^2/w_i^2\right)^{v_i/2}} = d\sigma^2 \frac{\exp\left(-\sqrt{\sum_{i=1}^d \rho_i^2 w_i^2/\xi_i^2}\right)}{\sum_{i=1}^d \left(1+\rho_i^2\right)^{v_i/2}} \ . \tag{5}$$

Class (B): Separable models

This class includes all separable covariance functions with one-dimensional components of the same functional form. In a coordinate system aligned with the principal axes these covariances are expressed as $c_x(\tilde{\mathbf{r}}) = \sigma_x^2 \prod_{i=1}^d g(\tilde{r}_i)$, where $g(\cdot)$ is a permissible one-dimensional covariance function (Christakos, 1992). Classes (A) and (B) are not completely disjoint since the Gaussian model belongs to both of them. However, with this notable exception, the models in Class (B) can not be reduced to isotropic functions. An example of a Class (B) covariance is the hole-effect model, defined by $g(\tilde{r}_i) = \sin(\tilde{r}_i)/\tilde{r}_i$.

Superellipsoidal covariance models

A new family of separable covariance models is defined based on geometrical generalizations of the ellipse called superellipsoids (Wallace, 1968). In two spatial dimensions a superellipsoid with index n obeys the following equation

$$|r_1/\xi_1|^{2/n} + |r_2/\xi_2|^{2/n} = |\tilde{r}_1|^{2/n} + |\tilde{r}_2|^{2/n} = c \ . \tag{6}$$

Let us define the following separable function

$$c_x(\tilde{\mathbf{r}}) = \sigma_x^2 g(|\tilde{r}_1|^{2/n}) g(|\tilde{r}_2|^{2/n}) \ . \tag{7}$$

We will define differentiability conditions for the random field and permissibility conditions for $c_x(\tilde{\mathbf{r}})$. Differentiability is partly determined by the index n. A Gaussian random field is everywhere differentiable (in the mean square sense) if the second-order derivative of the covariance exists at zero separation (e.g., Adler, 1981; Yaglom, 1987). The derivative at zero separation is given by (see Appendix 1)

$$\frac{\partial^2 c_x(\tilde{\mathbf{r}})}{\partial r_1^2} = \sigma_x^2 g(\omega_2) \left\{ \left[\frac{2}{n\xi_1} |\tilde{r}_1|^{2/n-1} \mathrm{sgn}(r_1) \right]^2 g''(\omega_1) + \frac{2g'(\omega_1)}{n\xi_1^2} \left(\frac{2}{n} - 1 \right) |\tilde{r}_1|^{2/n-2} \mathrm{sgn}^2(r_1) + \frac{4g'(\omega_1)}{n\xi_1^2} |\tilde{r}_1|^{2/n-1} \delta(r_1) \right\} \ . \tag{8}$$

In Eq. (8) the prime denotes the derivative with respect to $\omega_1 \equiv |r_1/\xi_1|^{2/n}$ and $\mathrm{sgn}(r_1)$ the sign function. The derivative at zero separation exists if the $g(\omega_1)$ is twice differentiable and the limits $\lim_{\omega_1 \to 0} g'(\omega_1)\omega_1^{2/n-2}$ and $\lim_{\omega_1 \to 0} g''(\omega_1)\omega_1^{4/n-2}$ exist. These conditions guarantee a finite covariance derivative.

Differentiability conditions: A superellipsoidal random field with covariance given by Eq. (7) is differentiable if (i) the function $g(\omega_1)$ is twice differentiable and (ii) $n \leq 1$ or $1 < n \leq 2$ and $g'(\omega_1)$ tends to zero faster than $\omega_1^{2-2/n}$.

The above conditions are not sufficient for permissibility. Permissibility criteria for a specific type of superellipsoidal covariance functions are derived below.

Exponential superellipsoid

Let us define the exponential superellipsoid

$$c_x(\mathbf{r}) = \sigma_x^2 \exp\left(-|r_1/\xi_1|^{2/n} - |r_2/\xi_2|^{2/n} \right) \ . \tag{9}$$

Except for $n = 1$ the functions defined by Eq. (9) do not reduce to an isotropic form. Hence, they differ from the exponential models $c_x(\mathbf{r}) = \sigma_x^2 \exp[-(r/\xi)^v]$ (Abrahamsen, 1997). The plots of the isolevel contours in Fig. 2 show clearly the departure from the ellipsoidal shape. The contours are rounded rectangles for $n < 1$, ellipses for $n = 1$, concave diamonds for $1 < n < 2$, diamonds for $n = 2$, and convex ("pinched") diamonds for $n > 2$. The exponential superellipsoid with index $n = 2$, was shown to be a permissible covariance function (Christakos et al., 2000). In general, it can be shown that the spectral density is non-negative for $\infty > n \geq 1$ (Schoenberg, 1938). In Fig. 3 we plot the spectral densities of the functions in Fig. 2, obtained with the Fast Fourier Transform method (e.g., Press et al., 1986). All densities are non-negative except for $n = 0.5$.

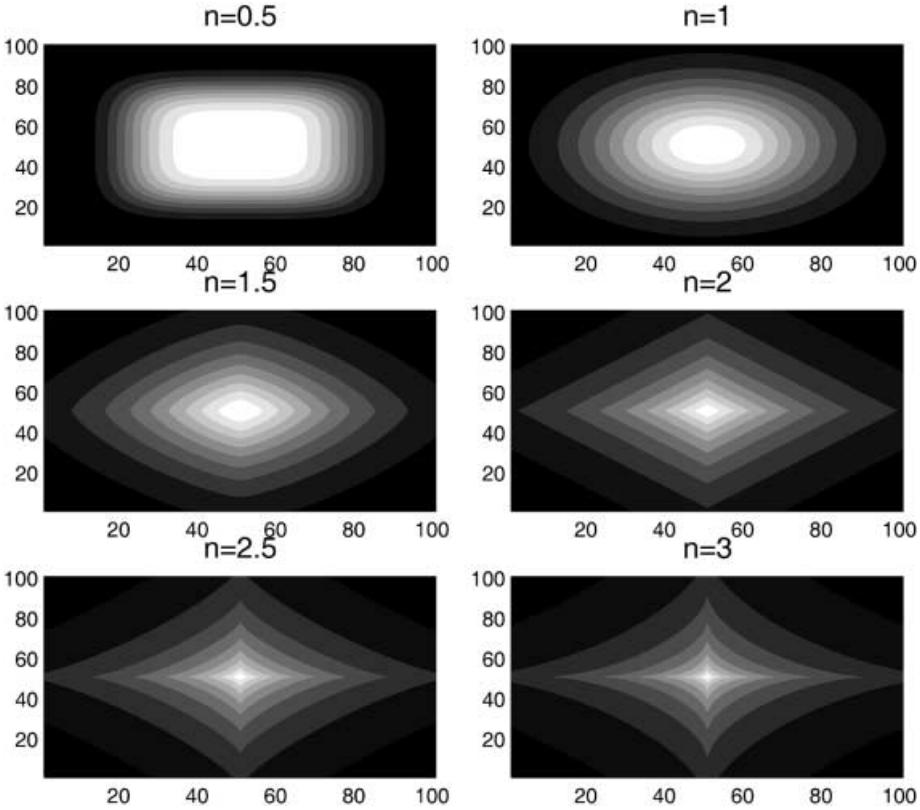

Fig. 2. Plot of the isolevel contours of the exponential superellipsoid functions for six values of the index $n = 0.5, 1, 1.5, 2, 2.5, 3$

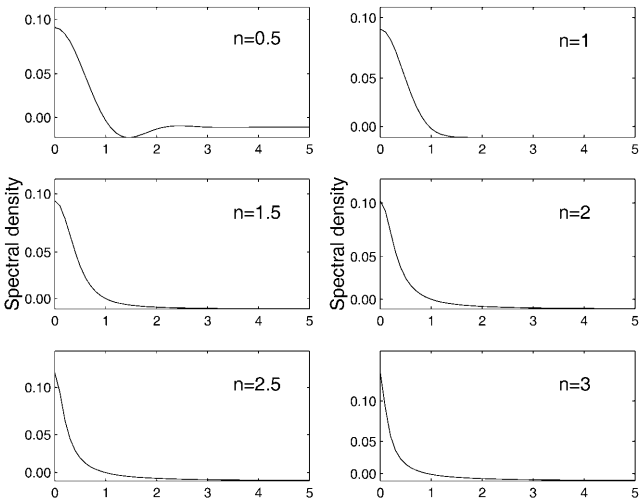

Fig. 3. Plot of the power spectral density for the exponential superellipsoid functions shown in Fig. 2

Permissibility condition: The exponential superellipsoids, defined by Eq. (9), are permissible covariances if $\infty > n \geq 1$. In view of the differentiability condition given above, the respective random fields are differentiable only for $n = 1$.

3
The covariance tensor identity

For differentiable random fields the second order derivatives of the covariance $\partial^2 c_x(\mathbf{h})/\partial h_i \partial h_j\big|_{h=0}$, generate the second-rank covariance tensor. The slope tensor (SRST) $X_{ij}(\mathbf{s})$ is defined by $X_{ij}(\mathbf{s}) = (\partial X(\mathbf{s})/\partial s_i)(\partial X(\mathbf{s})/\partial s_j)$. The mean value of $X_{ij}(\mathbf{s})$ is denoted by $\langle X_{ij}(\mathbf{s})\rangle \equiv Q_{ij}$ (the brackets denote the stochastic average). The mean SRST and the covariance tensor are related via the following tensor identity (e.g., Swerling, 1962)

$$Q_{ij} \equiv \left\langle \frac{\partial X(\mathbf{s})}{\partial s_i}\frac{\partial X(\mathbf{s})}{\partial s_j} \right\rangle = -\left.\frac{\partial^2 c_x(\mathbf{h})}{\partial h_i \partial h_j}\right|_{h=(0,0)} . \tag{10}$$

Equation (10) is not valid for non-differentiable random fields, e.g., for exponential covariance. The anisotropy parameters of non-differentiable fields can be estimated approximately using generalized derivatives (Yaglom, 1987; Christakos, 1992; Christakos and Hristopulos, 1998) as shown in Appendix 2. The covariance tensor identity permits estimating the anisotropic parameters from the mean SRST based on the available data. Then, it is possible to transform into a coordinate system in which the covariance function is either isotropic or a product of identical one-dimensional functions. The transformation involves a rotation that aligns the coordinate system with the principal axes, and a rescaling that makes all the correlation lengths equal. Standard geostatistical methods can be used (e.g., Christakos, 1992; Olea, 1999) to estimate the isotropic variogram in the transformed system. For a separable variogram it suffices to estimate one of its components along a principal direction. In either case there is no need to consider separately different directions in space. Once the variogram is estimated in the transformed system, the inverse set of transformations should be used to obtain the variogram in the original coordinate frame.

If ξ_i, $i = 1, \ldots, d$ denote the correlation lengths along the principal axes, $d-1$ *aspect ratios* can be defined as follows

$$R_{i(1)} \equiv \frac{\xi_1}{\xi_i}, \quad (i = 1, \ldots, d) \ . \tag{11}$$

The vector $\mathbf{R}_{(1)} = (1, R_{2(1)}, \ldots, R_{d(1)})$ has $d-1$ independent components. Below we determine the orientation of the principal axes and the correlation aspect ratio from the SRST. First, we consider a coordinate system aligned with the principal axes.

Principal axes coordinate system

We express the covariance function in terms of $\tilde{r}_i = r_i/\xi_i$. The covariance tensor identity leads to the following expression

$$Q_{ij} = -\frac{1}{\xi_i \xi_j}\left.\frac{\partial^2 c_x(\tilde{\mathbf{r}})}{\partial \tilde{r}_i \partial \tilde{r}_j}\right|_{r=(0,0)} \qquad (i, j = 1, \ldots, d) \tag{12}$$

In this system the covariance tensor for both Classes (A) and (B) models is isotropic at zero separation. Hence, $-\partial^2 c_x(\tilde{\mathbf{r}})/\partial\tilde{r}_i\partial\tilde{r}_j\big|_{r=(0,0)} \equiv \sigma_x^2\zeta^2\delta_{ij}$ for all i,j where ζ is a dimensionless number. The $d-1$ equations for the aspect ratios below follow from Eq. (12)

$$\sqrt{\frac{Q_{ii}}{Q_{11}}} = \frac{\xi_1}{\xi_i} = R_{i(1)}, \quad (i = 2, \ldots, d) \ . \tag{13}$$

The roots of the Eqs. (13) determine the correlation aspect ratios. Coordinate systems aligned with the principal axes are not always practical for applications. Nonetheless, such systems are useful for simulations and often a natural choice for engineered materials.

General coordinate system

Transformation of the covariance tensor to a system aligned with the principal axes involves the rotation matrix $\mathbf{U}$ (defined in Sect. 2). Using the chain rule for the derivatives of $c_x(\mathbf{h})$ we find $\partial c_x/\partial h_i = (\partial r_k/\partial h_i)\partial c_x/\partial r_k = U_{ki}\partial c_x/\partial r_k$ (summation is implied over repeated indices.) The rescaling transformation is based on $\partial c_x/\partial r_i = \xi_i^{-1}(\partial c_x/\partial\tilde{r}_i)$. Hence,

$$\frac{\partial^2 c_x}{\partial h_i \partial h_j} = \left(\frac{U_{ki}U_{lj}}{\xi_k\xi_l}\right)\frac{\partial^2 c_x}{\partial\tilde{r}_k\partial\tilde{r}_l} \ . \tag{14}$$

So, based on Eq. (12), the covariance tensor identity is expressed as follows

$$Q_{ij} = \frac{\sigma_x^2\zeta^2}{\xi_1^2}U_{ki}R_{k(1)}U_{lj}R_{l(1)}\delta_{kl} = \frac{\sigma_x^2\zeta^2}{\xi_1^2}U_{ki}U_{kj}R_{k(1)}^2, \quad (i,j = 1, \ldots, d) \ . \tag{15}$$

The expression (15) gives a system of equations with the components of the rotation matrix $\mathbf{U}$ and the vector $\mathbf{R}$ as unknowns. These should be determined from the mean SRST Q_{ij}. The constant ζ^2 and ξ_1^2 remain undetermined, but they are not needed for the rotation and rescaling transformations. The length ξ_1 is determined from the experimental variogram. The value of ζ^2 is not required in the variogram calculations, but it can be determined from the second-order derivative of the isotropic variogram (e.g., in the Gaussian case $\zeta^2 = 2$).

Two-dimensional random field

We derive specific expressions in two dimensions based on Eqs. (15). The rotation matrix $\mathbf{U}$ is given by $U_{11} = U_{22} = \cos\theta$ and $U_{12} = -U_{21} = \sin\theta$. The anisotropic ratio vector is $\mathbf{R}_{(1)} = (1, R_{2(1)})$. The Eqs. (15) are then expressed as follows

$$Q_{11} = \frac{\sigma_x^2\zeta^2}{\xi_1^2}\left(\cos^2\theta + R_{2(1)}^2\sin^2\theta\right) \ , \tag{16}$$

$$Q_{22} = \frac{\sigma_x^2\zeta^2}{\xi_1^2}\left(R_{2(1)}^2\cos^2\theta + \sin^2\theta\right) \tag{17}$$

$$Q_{12} = Q_{21} = \frac{\sigma_x^2 \zeta^2}{\xi_1^2} \left[\sin\,\theta \cos\,\theta (1 - R_{2(1)}^2) \right] \ . \tag{18}$$

The orientation of the principal axes is determined by θ and the aspect ratio by $R_{2(1)}$. By dividing both sides of Eqs. (17) and (18) by the terms on the respective sides of Eq. (16) we obtain the following set of equations

$$\frac{Q_{22}}{Q_{11}} = \left(\frac{R_{2(1)}^2 + \tan^2\,\theta}{1 + R_{2(1)}^2 \tan^2\,\theta} \right) \ , \tag{19}$$

$$\frac{Q_{12}}{Q_{11}} = \frac{\tan\theta (1 - R_{2(1)}^2)}{1 + R_{2(1)}^2\,\tan^2\theta} \ . \tag{20}$$

The roots of the non-linear system (19) and (20) are the anisotropic parameters. We define the following objective function

$$\Phi(\theta, R_{2(1)}) = \left[\frac{Q_{22}}{Q_{11}} - \left(\frac{R_{2(1)}^2 + \tan^2\theta}{1 + R_{2(1)}^2 \tan^2\theta} \right) \right]^2 + \left[\frac{Q_{12}}{Q_{11}} - \frac{\tan\theta (1 - R_{2(1)}^2)}{1 + R_{2(1)}^2\,\tan^2\theta} \right]^2 \ . \tag{21}$$

The function $\Phi(\theta, R_{2(1)})$ is non-negative and vanishes when both terms inside the brackets are zero. Hence, minimization of the objective function yields the anisotropic parameters (provided that the minimization does not stop at local minima).

4
Estimation of anisotropic parameters on regular grids

In this section we discuss the estimation of the mean SRST and the anisotropic parameters from data distributed on a regular grid. Regularly distributed data are not the rule in environmental applications. However, uniform spacing is useful for laboratory studies of porous materials (e.g., Henriette et al., 1989) and simulations. In practice, the derivative operators in $X_{ij}(\mathbf{s})$ are replaced by discrete differences. An accurate estimate $\hat{X}_{ij}(\mathbf{s})$ that closely approximates $\langle X_{ij}(\mathbf{s}) \rangle$ requires small discretization step (compared to the correlation length). Precision measures the uncertainty of $\hat{X}_{ij}(\mathbf{s})$, and it improves with increasing domain size (for fixed correlation length). We assume that $X(\mathbf{s})$ data are distributed on a Cartesian grid G with N points at the locations $\mathbf{s}_k$ $(k = 1, \ldots, N)$. The mean SRST $\hat{Q}_{ij}$ is estimated based on the forward-difference operator as follows

$$\hat{Q}_{ij} = \frac{1}{N b_i b_j} \sum_{k=1}^{N} \left[X(\mathbf{s}_k + b_i \hat{\mathbf{e}}_i) - X(\mathbf{s}_k) \right] \left[X(\mathbf{s}_k + b_j \hat{\mathbf{e}}_j) - X(\mathbf{s}_k) \right] \ . \tag{22}$$

The discretization step is b_i and $\hat{\mathbf{e}}_i$ denotes the unit vector in direction s_i. The right hand-side of Eq. (22) can be calculated very efficiently numerically. Estimation of the anisotropic parameters is based on the solution of the Eqs. (15). In two dimensions this is equivalent to the minimization of the objective function (21). We illustrate the numerical procedures using synthetic random field examples.

Numerical example

We generate random fields with $\sigma_x^2 = 1$, $\xi_1 = 6$, $\xi_2 = 4$ and Gaussian covariance ($\zeta^2 = 2$) on a square grid with L nodes per side, aligned with the principal anisotropy axes. According to Eq. (10) the SRST is given in this system by

$$\mathbf{Q} = 2\sigma_x^2 \begin{bmatrix} \xi_1^{-2} & 0 \\ 0 & \xi_2^{-2} \end{bmatrix} . \tag{23}$$

We use the Fourier Filtering Method (FFM) (e.g., Makse et al., 1996b; Le Ravalec et al., 2000) for the simulations. The "true" values of the mean SRST tensor are $Q_{11} = 0.0556$ and $Q_{22} = 0.1250$. The anisotropic ratio is $R_{2(1)} = 1.5$. One realization of the field for $L = 100$ is shown in Fig. 4. In Fig. 5 we plot the estimated SRST components and the aspect ratio $R_{2(1)}$ as functions of L. The SRST components approach stable values for $L > 100$. The aspect ratio levels off faster. The difference is probably due to fluctuations of the sample variance. The SRST depends on the variance, while the aspect ratio is, in contrast, independent.

Next, we calculate the SRST for random fields with principal axes rotated by 45°. A sample plotted in Fig. 6 shows clearly the tilting of the axes. Three different realizations with the same aspect ratio and orientation angle ($R_{2(1)} = 1.5$ and $\theta = 45°$) but different correlation lengths are generated. We estimate the SRST elements numerically from Eq. (22) and use them in Eq. (21) to estimate the anisotropic parameters by minimizing the objective function $\Phi(\theta, R_{2(1)})$. For the minimization we use an algorithm based on the simplex search method of Nelder and Mead (e.g., Press et al., 1986). We initialize the search with values $\theta_0 = 0°$ and $R_{2(1)} = 1$. The results for the mean SRST and the anisotropic parameters are shown in Table 1. The table also lists the theoretical values of the mean SRST, obtained from Eqs. (16) to (18). The estimates of the anisotropic parameters are accurate, especially for the fields with smaller correlation lengths. As the correlation length increases the accuracy of the estimates is reduced due to the finite size of the sample. The maximum aspect ratio that can be accurately estimated depends on the domain size since ergodic estimates require $\xi_{\max} \ll L$.

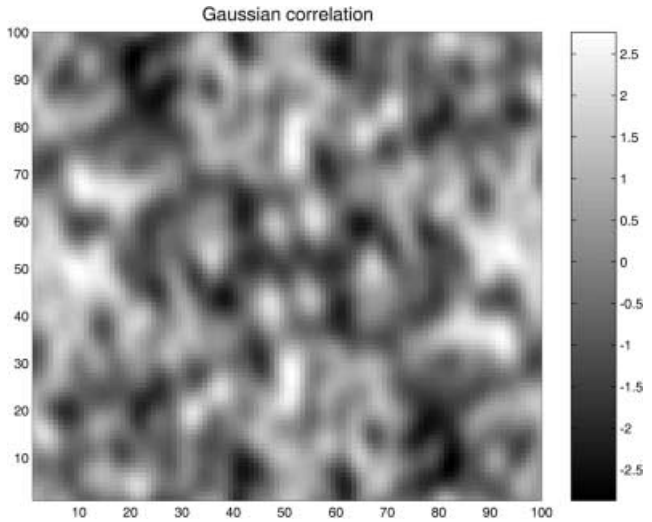

Fig. 4. Plot of a two-dimensional random field with anisotropic Gaussian covariance, $\sigma_x = 1$, $\xi_1 = 6$, $\xi_2 = 4$. The principal axes coincide with the axes of the coordinate system

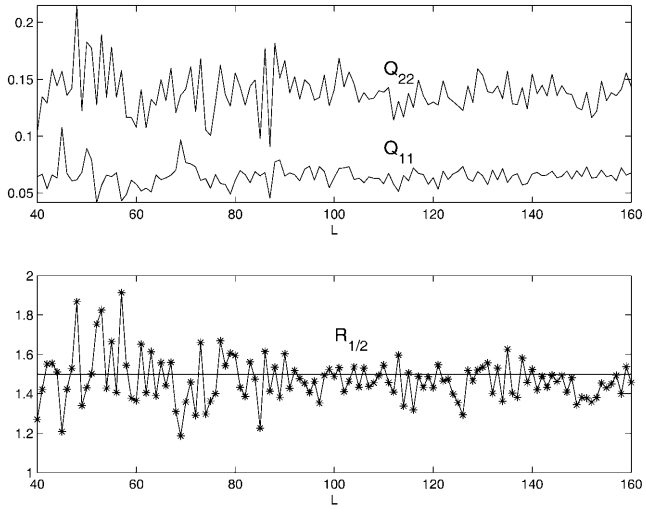

Fig. 5. Plot of the diagonal elements of the SRST and the anisotropic ratio as a function of the system size for sizes in the range between 40 and 161 nodes per side

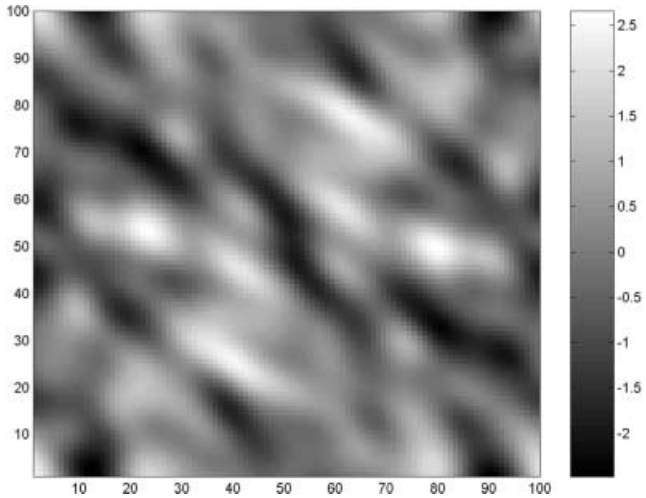

Fig. 6. Plot of a two-dimensional random field with Gaussian covariance, $\sigma_x = 1$, $\xi_1 = 7.5$ and $\xi_2 = 5$. The principal axes are rotated by 45° with respect to the coordinate system

Assuming that $L \geq 20\xi_{\max}$ to satisfy ergodic requirements, the maximum aspect ratio should be $R_{\max} \leq L/20\xi_{\min}$. The estimates of the mean SRST elements are not as accurate as the anisotropic parameters, most likely due to fluctuations of the sample variance, as we discussed above.

5
Estimation of anisotropic parameters from sparse data

Spatially sparse data sets routinely occur in geostatistical applications. Let us use $r_{\mathrm{nn}}(\mathbf{s}_k) = \left\|\mathbf{s}_{\mathrm{nn}(k)} - \mathbf{s}_k\right\|$ to denote the distance between the datum at point $\mathbf{s}_k$ and

Table 1. Estimates and theoretical values of the mean SRST, the aspect ratio and the orientation angle of the principal axes (in degrees). Three realizations of a two-dimensional random field with different correlation lengths are investigated. The theoretical aspect ratio is 1.5 and the orientation angle 45° for all the realizations

	Q_{11}	Q_{22}	Q_{12}	$R_{2(1)}$	θ
$\xi_1 = 4.5, \xi_2 = 3$					
Estimated	0.1132	0.1250	−0.0441	1.48	41.18
Theoretical	0.1605	0.1605	−0.0617	1.50	45
$\xi_1 = 7.5, \xi_2 = 5$					
Estimated	0.0475	0.0486	−0.0193	1.53	44.17
Theoretical	0.0578	0.0578	−0.022	1.50	45
$\xi_1 = 15, \xi_2 = 10$					
Estimated	0.0130	0.0147	−0.0037	1.32	38.46
Theoretical	0.0144	0.0144	−0.0056	1.50	45

its nearest neighbor. Let $r_{\mathrm{nn,max}} = \max[r_{\mathrm{nn}}(\mathbf{s}_k)]$ $(k = 1, \ldots, N)$ be the maximum nearest-neighbor distance. A data set is dense if the *index* $\mu_{\mathrm{de}} = \xi_{\min}/r_{\mathrm{nn,max}}$, $\xi_{\min} = \min(\xi_i)$ $(i = 1, \ldots, d)$ is larger than one. Large values of μ_{de} permit more accurate estimation of the derivatives, but this should be balanced against the danger of local numerical instabilities due to very small $r_{\mathrm{nn}}(\mathbf{s}_k)$. The data distribution is *uniform* if $r_{\mathrm{nn}}(\mathbf{s}_k)$ varies little from site to site. The variation is measured by the *uniformity index* $\mu_{\mathrm{un}} = \overline{r_{\mathrm{nn}}}/\sqrt{\mathrm{Var}(r_{\mathrm{nn}})}$. Low values of μ_{un} indicate high variability. Various approximate estimators of the SRST can be defined for irregularly spaced data. If we use the Euclidean distance, the discretization step at $\mathbf{s}_k$ in the direction s_i is given by $\Delta s_{k,i} = s_{\mathrm{nn}(k),i} - s_{k,i}$. Large steps have a smoothening effect on the slope, while very small steps lead to large numerical fluctuations. Hence, the point $\mathbf{s}_k$ will be included in the estimation of $\hat{Q}_{ij}$ if the $|\Delta s_{k,i}|$ and $|\Delta s_{k,j}|$ are bounded inside $[\alpha_{\mathrm{l}}, \alpha_{\mathrm{u}}]$. If $\mathbf{s}^*_k$ denote the locations and $N_{\mathrm{eff}}(i,j)$ the number of data points used in the calculation of $\hat{Q}_{ij}$, this is given by

$$\hat{Q}_{ij} = \frac{1}{N_{\mathrm{eff}}(i,j)} \sum_{k=1}^{N_{\mathrm{eff}}(i,j)} \left[\frac{X(\mathbf{s}^*_{\mathrm{nn}(k)}) - X(\mathbf{s}^*_k)}{\Delta s^*_{k,i}}\right] \left[\frac{X(\mathbf{s}^*_{\mathrm{nn}(k)}) - X(\mathbf{s}^*_k)}{\Delta s^*_{k,j}}\right] . \tag{24}$$

The cutoffs α_{l} and α_{u} are not a priori specified. To avoid excessive smoothing the upper cutoff should satisfy $\alpha_{\mathrm{u}} \ll \xi_{\min}$, but $\xi_{\min}$ is indeterminate before calculation of the variogram. An initial estimate can be obtained by visual inspection of approximate maps of the data. On the other hand, $\alpha_{\mathrm{l}}/\xi_{\min}$ should not be too small, because noise would dominate the estimate of the slopes.

Numerical example

We illustrate the calculation of the SRST for a sparse data distribution. We simulate a field at N random sites within a square domain of length L using the harmonic superposition method (Drummond, 1987; Jinnai et al., 2000). This is less efficient than the FFM, but it can generate field values at any location. The superposition is defined by

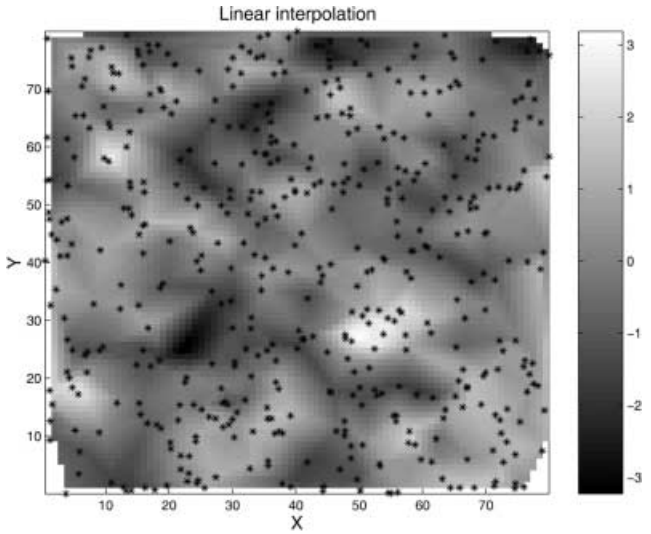

Fig. 7. Grayscale map of a sparsely sampled random field. The positions of the "data points" are marked with stars. The map was generated from the available data using linear interpolation

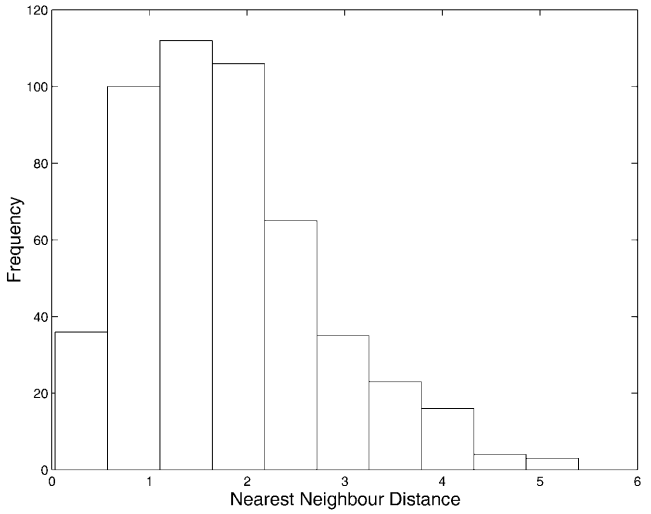

Fig. 8. Histogram of the nearest-neighbor distances for the data set of Fig. 7

$$X(\mathbf{s}) = \sigma_x \left(\frac{2}{N_\mathrm{m}}\right)^{1/2} \sum_{n=1}^{N_\mathrm{m}} \cos(\mathbf{k}_n \cdot \mathbf{s} + \phi_n) \quad . \tag{25}$$

The phase variables ϕ_n are distributed uniformly in $[0, 2\pi]$. The wavevectors $\mathbf{k}_n$ are randomly distributed with probability density $f_\mathrm{x}(\mathbf{k}_n) = A\tilde{c}_x(\mathbf{k}_n)$, where $\tilde{c}_x(\mathbf{k}_n)$ is the spectral density of the covariance $c_x(\mathbf{r})$ and $A = \left[\int \mathrm{d}\mathbf{k}_n \tilde{c}_x(\mathbf{k}_n)\right]^{-1}$. For a Gaussian $c_x(\mathbf{r})$ the normalized spectral density is $f_\mathrm{x}(\mathbf{k}_n) = (\xi_1\xi_2/4\pi)\exp$

Table 2. Estimates of the mean SRST tensor and the number of sites used in the calculation of each element for different values of the lower cutoff with a fixed upper cutoff $\alpha_u = 2$. The theoretical values of the mean SRST elements are $Q_{11} = 0.1250$, $Q_{22} = 0.0556$ and $Q_{12} = 0$

α_l	$\hat{Q}_{11}$	$\hat{Q}_{22}$	$\hat{Q}_{12}$	$N_{\text{eff}}(1,1)$	$N_{\text{eff}}(2,2)$	$N_{\text{eff}}(1,2)$
0.1	15.237	28.232	−0.109	424	420	359
0.2	1.508	0.584	0.002	380	385	298
0.3	0.703	0.442	−0.005	355	368	265
0.4	0.653	0.336	−0.033	323	334	216
0.5	0.466	0.229	−0.039	295	309	180
0.6	0.303	0.218	−0.056	263	282	141
0.7	0.298	0.193	−0.052	241	255	110
0.8	0.281	0.175	−0.060	192	202	69
0.9	0.172	0.139	−0.034	169	171	55
1.0	0.161	0.132	−0.005	156	154	40
1.1	0.150	0.121	−0.041	137	129	31
1.2	0.152	0.084	0.008	125	99	17
1.3	0.143	0.084	−0.002	99	84	12
1.4	0.141	0.074	0.009	84	68	8
1.5	0.151	0.078	−0.020	74	52	6

$\left[-\left(k_1^2\xi_1^2 + k_2^2\xi_2^2\right)/4\right]$. Based on the normalized central limit theorem the superposition tends to the normal distribution as N_{m} tends to infinity.

We simulate the data set using 500 random sites on a 80×80 square domain. The random field has $\sigma_x = 1$, $\xi_1 = 4$, $\xi_2 = 6$, and principal axes aligned with the domain sides. The corresponding mean SRST values according to Eq. (23) are $Q_{11} = 0.1250$, $Q_{22} = 0.0556$, and $Q_{12} = 0$. The number of modes used in the simulation is $N_{\text{m}} = 14000$. A map of the simulated data set is shown in Fig. 7. The plotted values on the regular grid were obtained from the field values at the random sites by linear interpolation. Figure 8 shows a histogram of the nearest-neighbor distance distribution $r_{\text{nn}}(s_k)$. The uniformity index is $\mu_{\text{un}} \cong 1.83$ based on $\overline{r_{\text{nn}}(\mathbf{s}_k)} \cong 1.79$ and $\sqrt{\text{Var}(r_{\text{nn}})} \cong 0.98$. The maximum nearest-neighbor distance is $r_{\text{nn,max}} \cong 5.40$ giving a density index $\mu_{\text{de}} \cong 0.56$. Hence, the "data set" is fairly uniform but not very dense. In Table 2 we show the estimates of the SRST components for different values of α_l. The upper cutoff is $\alpha_u = 2$ (one half of ξ_{min}). The best agreement with the theoretical SRST values is obtained for $\alpha_l \in [1 - 1.5]$. However, $N_{\text{eff}}(i,j)$ is small for these values of α_l, implying reduced precision. The sparseness of the data set imposes strong constraints on predictability. This is an inherent limitation of spatial statistics analyses when the size of the available data set is small.

6
Conclusions and discussion

This paper focuses on the modeling of range anisotropy in spatial statistics. We present a truncated power-law covariance with short and long-range cutoffs, which has applications in subsurface hydrology. We also introduce a family of separable covariances based on superellipsoids. These functions are useful for non-Euclidean metric spaces and have non-elliptical isolevel contours. We also propose a new method for estimating the anisotropic parameters of random fields. This method is based on the covariance tensor identity and employs the mean SRST, which can be estimated from the available data. We formulate a

system of equations that relate the mean SRST to the anisotropic parameters in any number of dimensions. In two spatial dimensions we derive an explicit system of nonlinear equations for the anisotropic parameters, which we solve by minimizing an appropriate objective function. We calculate the mean SRST and the anisotropic parameters using simulated random fields with both regular and sparse distributions. Extension of the method to three dimensions is straightforward, based on the general equations (15). We are also investigating a different approach for solving the nonlinear system based on a globally convergent Newton method.

Estimation of the mean SRST from sparse distributions merits further investigation, especially the cutoffs used in the calculation of the field derivatives. An alternate approach is to define nearest neighbors separately in each direction. Next nearest neighbors can be considered if the distance between two nearest neighbors is smaller than the lower cutoff. It is possible to estimate the mean SRST using maximum likelihood methods (e.g., Kitanidis, 1983). However, this will not eliminate the numerical issues related to the calculation of the random field gradients so long as they are involved in the observation set of the likelihood function.

Appendix 1

We calculate the second partial derivative of the covariance $c_x(\tilde{\mathbf{r}}) = \sigma_x^2 g(|\tilde{r}_1|^{2/n}) g(|\tilde{r}_2|^{2/n})$ with respect to r_1. Let us define $\omega_i \equiv |r_i/\xi_i|^{2/n}$ $(i = 1, 2)$. The first partial derivative is

$$\partial c_x(\tilde{\mathbf{r}})/\partial r_1 = \sigma_x^2 g(\omega_2) \mathrm{d}g(\omega_1)/\mathrm{d}r_1 \quad . \tag{1.1}$$

Since $\mathrm{d}\omega_i/\mathrm{d}r_i = (2/n\xi_i)|r_i/\xi_i|^{2/n-1}\mathrm{sgn}(r_i)$, where $\mathrm{sgn}(\cdot)$ is the sign function, we obtain

$$\mathrm{d}g(\omega_1)/\mathrm{d}r_1 = g'(\omega_1)\mathrm{d}\omega_1/\mathrm{d}r_1 = \left[2g'(\omega_1)|r_1/\xi_1|^{2/n-1}/n\xi_1\right]\mathrm{sgn}(r_1) \tag{1.2}$$

where $g'(\omega_i) = \mathrm{d}g(\omega_i)/\mathrm{d}\omega_i$. Similarly, the second partial derivative is given by

$$\frac{\partial^2 c_x(\tilde{\mathbf{r}})}{\partial r_1^2} = \sigma_x^2 g(\omega_2) \frac{\mathrm{d}^2 g(\omega_1)}{\mathrm{d}r_1^2} = \sigma_x^2 g(\omega_2) \frac{\mathrm{d}}{\mathrm{d}r_1}\left[\frac{2g'(\omega_1)}{n\xi_1}\left|\frac{r_1}{\xi_1}\right|^{2/n-1}\mathrm{sgn}(r_1)\right] \tag{1.3}$$

The derivative of the bracketed term on the right hand side of Eq. (1.3) is given by

$$\begin{aligned}\frac{\mathrm{d}}{\mathrm{d}r_1}\left[\frac{2g'(\omega_1)}{n\xi_1}\left|\frac{r_1}{\xi_1}\right|^{2/n-1}\mathrm{sgn}(r_1)\right] &= \left[\frac{2}{n\xi_1}\left|\frac{r_1}{\xi_1}\right|^{2/n-1}\mathrm{sgn}(r_1)\right]^2 g''(\omega_1) \\ &\quad + \frac{2g'(\omega_1)}{n\xi_1^2}\left(\frac{2}{n}-1\right)\left|\frac{r_1}{\xi_1}\right|^{2/n-2}\mathrm{sgn}^2(r_1) \\ &\quad + \frac{4g'(\omega_1)}{n\xi_1^2}\left|\frac{r_1}{\xi_1}\right|^{2/n-1}\delta(r_1) \quad ,\end{aligned} \tag{1.4}$$

where we used $\partial \mathrm{sgn}(r_1)/\partial r_1 = 2\delta(r_1)$. Finally, we obtain

$$\frac{\partial^2 c_x(\tilde{\mathbf{r}})}{\partial r_1^2} = \sigma_x^2 g(\omega_2)\left\{\left[\frac{2}{n\xi_1}\left|\frac{r_1}{\xi_1}\right|^{2/n-1}\mathrm{sgn}(r_1)\right]^2 g''(\omega_1)\right.$$

$$\left. + \frac{2g'(\omega_1)}{n\xi_1^2}\left(\frac{2}{n}-1\right)\left|\frac{r_1}{\xi_1}\right|^{2/n-2}\mathrm{sgn}^2(r_1) + \frac{4g'(\omega_1)}{n\xi_1^2}\left|\frac{r_1}{\xi_1}\right|^{2/n-1}\delta(r_1)\right\} \ . \tag{1.5}$$

Appendix 2

The covariance tensor identity is not valid for non-differentiable random fields (e.g., for exponential covariance dependence). However, the identity can be extended to *generalized random fields* that are differentiable. Assume that $\Phi(\mathbf{s}-\mathbf{s}')$ is a real, differentiable kernel and define the generalized random field $X_\Phi(\mathbf{s})$ as follows

$$X_\Phi(\mathbf{s}) = \int \mathbf{ds}'\Phi(\mathbf{s}-\mathbf{s}')X(\mathbf{s}') = \int \mathbf{dw}\Phi(\mathbf{w})X(\mathbf{s}-\mathbf{w}) \ . \tag{2.1}$$

Then, the partial derivatives $\partial X_\Phi(\mathbf{s})/\partial s_i$ $(i=1,\ldots,d)$ are defined by

$$\frac{\partial X_\Phi(\mathbf{s})}{\partial s_i} = \int \mathbf{ds}'\frac{\Phi(\mathbf{s}-\mathbf{s}')}{\partial s_i}X(\mathbf{s}') = \int \mathbf{dw}\frac{\Phi(\mathbf{w})}{\partial w_i}X(\mathbf{s}-\mathbf{w}) \ . \tag{2.2}$$

The generalized covariance of the field $X_\Phi(\mathbf{s})$ is

$$c_{x,\Phi}(\mathbf{h}) \equiv \langle X_\Phi(\mathbf{s})X_\Phi(\mathbf{s}+\mathbf{h})\rangle = \int \mathbf{dy}\Psi(\mathbf{y})c_x(\mathbf{h}-\mathbf{y}) \ . \tag{2.3}$$

The kernel of the convolution is $\Psi(\mathbf{s}) = \alpha\int \mathbf{dz}\Phi[(\mathbf{z}+\mathbf{y})/2)]\Phi[(\mathbf{z}-\mathbf{y})/2)]$ where α is the constant Jacobian of the transformation to the center-of-mass coordinate system. The covariance tensor identity is then valid for the differentiable field $X_\Phi(\mathbf{s})$.

To determine the anisotropic parameters with accuracy, the kernel function should not affect significantly the anisotropy of the original field. Ideally, the function $\Psi(\mathbf{y})$ should have the same anisotropic dependence as $X(\mathbf{s})$. However, this is not possible in practice, since the anisotropy of $X(\mathbf{s})$ is unknown. Instead, we can use a short-range isotropic kernel, which disturbs only minimally the anisotropy. Without loss of generality, we express the covariance tensor identity in the principal axes system in terms of Fourier transforms

$$Q_{ij}^\Phi = \int \frac{\mathbf{dk}}{(2\pi)^d}k_i k_j \tilde{c}_x(\mathbf{k})\tilde{\Psi}(\mathbf{k}) \quad (i,j=1,\ldots,d) \ . \tag{2.4}$$

The $\tilde{\Psi}(\mathbf{k})$ is a function of the dimensionless variable $k\ell$, where ℓ is the range of the isotropic kernel. By using the dimensionless variables $u_i = k_i\xi_i$ $(i=1,\ldots,d)$, we obtain

$$Q_{ij}^{\Phi} = \frac{1}{\xi_i \xi_j (2\pi)^d} \int \mathbf{du} u_i u_j \tilde{c}'_x(\mathbf{u}) \tilde{\Psi}'(u_1 \ell/\xi_1, \ldots, u_d \ell/\xi_d) \ , \tag{2.5}$$

where $\tilde{c}'_x(\mathbf{u})$ is the isotropic function obtained from $\tilde{c}_x(\mathbf{k})$ by rescaling, and $\tilde{\Psi}'(u_1 \ell/\xi_1, \ldots, u_d \ell/\xi_d)$ is the function, in general anisotropic, obtained from $\tilde{\Psi}(\mathbf{k})$. If $\ell/\xi_i \ll 1$ $(i = 1, \ldots, d)$, the Eq. (2.5) can be approximated as follows

$$Q_{ij}^{\Phi} \cong \frac{\tilde{\Psi}'(0)}{\xi_i \xi_j (2\pi)^d} \int \mathbf{du} u_i u_j \tilde{c}'_x(\mathbf{u}) = \frac{\tilde{\Psi}'(0)}{\xi_i \xi_j (2\pi)^d} \frac{\delta_{ij}}{d} \int_0^{\infty} \mathrm{d}u u^{d-1} \tilde{c}'_x(u) \ , \tag{2.6}$$

where δ_{ij} is the Kronecker delta and $\tilde{\Psi}'(0) = \tilde{\Psi}'(u = 0)$. Based on Eq. (2.6) we obtain the equivalent of Eq. (13) as follows

$$\sqrt{\frac{Q_{ii}^{\Phi}}{Q_{11}^{\Phi}}} \cong \frac{\xi_1}{\xi_i} \quad (i = 1, \ldots, d) \ . \tag{2.7}$$

References

Abrahamsen P (1997) A review of Gaussian random fields and correlation functions. Rapport No. 917, SAND, Norwegian Computing Center, Oslo, Norway

Adler RJ (1981) The Geometry of Random Fields. John Wiley & Sons, New York, NY, USA

Bochner S (1959) Lectures on Fourier Integrals. Princeton University Press, Princeton, NJ, USA

Bouchaud JP, Georges A (1990) Anomalous diffusion in disordered media, Statistical mechanics, models and physical applications. Phys. Rep. 195: 127–293

Chaikin PM, Lubensky TC (1995) Principles of Condensed Matter Physics. Cambridge University Press, New York, NY, USA

Choy D, Chen S (2000) Clipped random wave analysis of isomeric lamellar microemulsions. Phys. Rev. E 61(4): 4148–4155

Christakos G (1992) Random Field Models in Earth Sciences. Academic Press, San Diego, CA, USA

Christakos G (2000) Modern Spatiotemporal Geostatistics. Oxford University Press, New York, NY, USA

Christakos G, Hristopulos DT (1998) Spatiotemporal Environmental Health Modelling: A Tractatus Stochasticus. Kluwer Academic Publishers, Boston, MA, USA

Christakos G, Hristopulos DT, Bogaert P (2000) On the physical geometry concept at the basis of space/time geostatistical hydrology. Adv. Water Resour. 23(8): 799–810

Cushman JH (1984) On unifying the concepts of scale, instrumentation and stochastics in the development of multiphase transport theory. Water Resour. Res. 20(11): 1668–1676

Cushman JH (1986) On measurement, scale and scaling. Water Resour. Res. 22(2): 129–134

Drummond IT, Horgan RR (1987) The effective permeability of a random medium. J. Phys. A 20: 4661–4672

Di Federico V, Neuman SP (1997) Scaling of random fields by means of truncated power variograms and associated spectra. Water Resour. Res. 33(5): 1075–1085

Di Federico V, Neuman SP (1998) Flow in multiscale log-conductivity fields with truncated power variograms. Water Resour. Res. 34(5): 975–987

Erikson M, Siska P (2000) Understanding anisotropy computations. Math. Geol. 32(6): 683–700

Feder J (1988) Fractals. Plenum Press, New York, NY, USA

Gelhar LW (1993) Stochastic Subsurface Hydrology. Prentice Hall, Englewood Cliffs, NJ, USA

Gradshteyn IS, Ryzhik IM (1994) Tables of Integrals, Series, and Products (5th edn). Academic Press, New York, NY, USA

Henriette A, Jacquin CG, Adler PM (1989) The effective permeability of heterogeneous porous media. PhysicoCh. Hydrodyn. 11(1): 63–79
Isichenko MB (1992) Percolation, statistical topography, and transport in porous media. Rev. Mod. Phys. 64(4): 961–1043
Jinnai H, Nishikawa Y, Spontak SD, Smith RJ, Agard DA, Hashimoto T (2000a) Direct measurement of interfacial curvature distributions in a bicontinuous block copolymer morphology. Phys. Rev. Let. 84(3): 518–521
Jinnai H, Nishikawa Y, Chen S, Koizumi S, Hashimoto T (2000b) Morphological characterization of bicontinuous structures in polymer blends and microemulsions by the inverse-clipping method in the context of the clipped-random-wave model. Phys. Rev. E 61(6): 6773–6780
Kikkinides ES, Burganos VN (1999) Structural and flow properties of binary media generated by fractional Brownian motion models. Phys. Rev. E 59(6): 7185–7194
Kikkinides ES, Burganos VN (2000) "Permeation properties of three-dimensional self-affine reconstructions of porous materials. Phys. Rev. E 62(5): 6906–6915
Kitanidis PK (1983) Statistical estimation of polynomial generalized covariance functions and hydrologic applications. Water Resour. Res. 19: 909–921
Koch DL, Brady JF (1988) Anomalous diffusion in heterogeneous porous media. Phys. Fluids A 31(1): 965–973
Le Ravalec M, Noettinger B, Hu LY (2000) The FFT Moving Average (FFT-MA) Generator: an efficient numerical method for generating and conditioning Gaussian simulations. Math. Geol. 32(6): 701–724
Liu HH, Molz FJ (1997) Comment on 'Evidence for non-Gaussian scaling behavior in heterogeneous sedimentary formations' by S. Painter. Water Resour. Res. 33(4): 907–908
Molz FJ, Liu HH, Szulga J (1997) Fractional Brownian motion and fractional Gaussian noise in subsurface hydrology: a review, presentation of fundamental properties, and extensions. Water Resour. Res. 33(10): 2273–2286
Lovejoy S, Schertzer D (1995) Multifractals and rain. In Kundzevicz AW (ed) New Uncertainty Concepts in Hydrology and Hydrological Modeling, pp. 61–103. Cambridge University Press, New York, NY, USA
Makse HA, Davies GW, Havlin S, Ivanov PC, King PR, Stanley HE (1996a) Long-range correlations in permeability fluctuations in porous rock. Phys. Rev. E 54(4): 3129–3134
Makse HA, Havlin S, Schwartz M, Stanley HE (1996b) Method for generating long-range correlations for large systems. Phys. Rev. E 53(5): 5445–5449
Mandelbrot BB (1982) The Fractal Geometry of Nature. Freeman and Company, New York, NY, USA
Mandelbrot BB, Van Ness JW (1968) Fractional Brownian motions, fractional noises and applications. SIAM Review 10(4): 422–437
Menadbe M, Seed A, Harris D, Austin G (1999) Multiaffine random field model of rainfall. Water Resour. Res. 35(2): 509-514
Neuman SP (1990) Universal scaling of hydraulic conductivities and dispersivities in geologic media. Water Resour. Res. 26(8): 1749-1758
Neuman SP (1994) Generalized scaling of permeabilities, validation and effect of support scale. Geoph. Rev. Let. 21(5): 349–352
Olea RA (1999) Geostatistics for Engineers and Earth Scientists. Kluwer Academic Publishers, Boston, MA, USA
Painter S (1996) Evidence for non-Gaussian scaling behavior in heterogeneous sedimentary formations. Water Resour. Res. 32(5): 1323–1332
Provatas N, Alava MJ, Ala-Nissila T (1996) Density correlations in paper. Phys. Rev. E 54(1): R36–R38
Press WH, Flannery BP, Teukolsky SA, Vettering WT (1986) Numerical Recipes. Cambridge University Press, New York, NY, USA
Schertzer D, Lovejoy S (1987) Physically based rain and cloud modeling by anisotropic, multiplicative turbulent cascades. J. Geophys. Res. 92: 9692–9714
Schoenberg IJ (1938) Metric spaces and positive definite functions. Trans. Amer. Math. Soc. 44(3): 522–536
Swerling P (1962) Statistical properties of the contours of random surfaces. IRE Trans. Infor. Th. IT-8: 315–321

Veneziano D, Bras RL, Niemann JD (1996) Nonlinearity and self-similarity of rainfall in time and a stochastic model. J. Geophys. Res. Atmos. 101(D21): 26371–26392
Wallace A (1968) Differential Topology. Benjamin/Cummings, Reading, MA, USA
Yaglom AM (1987) Correlation Theory of Stationary and Related Random Functions I. Springer Series in Statistics, Springer, New York, NY, USA